ChemComm

COMMUNICATION

View Article Online
View Journal | View Issue

Cite this: *Chem. Commun.*, 2015, 51, 13279

Received 30th May 2015,
Accepted 13th July 2015

DOI: 10.1039/c5cc04434k

www.rsc.org/chemcomm

High-rate performance of a mixed olivine cathode with off-stoichiometric composition†

Jae Chul Kim,[a] Xin Li,[a] Byoungwoo Kang[b] and Gerbrand Ceder*[ac]

We highlight that the off-stoichiometric compositional variation is a simply effective method to improve the power density of $LiFe_{0.6}Mn_{0.4}PO_4$. This strategy does not require a supplementary separate coating and is likely applicable to other compositions given the feasibility of the method.

Superior operating safety with long cycle life and low material cost makes lithium iron phosphate ($LiFePO_4$) an important Li storage material.[1–3] For this olivine compound, many efforts have been expended in order to achieve desirable electrochemical properties such as particle nanosizing and applying electrically conductive coating.[4–8] However, these processes reduce tap density and therefore lower practical energy density,[9] making the material lose much of its appeal toward commercialization as compared to current oxide-based cathodes.[10,11] Thus, enhancing the energy density of nanosized and coated $LiFePO_4$ is an important problem for battery scientists and engineers.

Higher theoretical energy density for $LiFePO_4$ can be achieved by mixing Mn with Fe, taking advantage of the $Mn^{2+/3+}$ redox potential at 4.1 V over $Fe^{2+/3+}$ at 3.4 V.[12–15] It is also reported that Mn substitution can alter the delithiation mechanism from phase separation to a solid solution reaction.[16–18] Compositions with large Mn content, however, tend to lack reasonable rate performance.[19–21] In this communication, we present a simple and efficient method to enable high rate capability of the mixed olivine cathode, $LiFe_{0.6}Mn_{0.4}PO_4$, by controlling off-stoichiometry to create an electrically conductive glassy coating. This concept is previously established in $LiFePO_4$,[22] and the effectiveness to achieve high power density has also been demonstrated in other cathode materials.[23–27] The molar ratio of the off-stoichiometric composition is 1 : 0.9 : 0.95 for Li : ($Fe_{0.6}$ + $Mn_{0.4}$) : P, as optimized previously,[22,23] so that the nominal composition becomes $LiFe_{0.54}Mn_{0.36}P_{0.95}O_{4-\delta}$. The experimental details of synthesis, characterization, and electrochemistry are summarized in ESI.†

Fig. 1a shows the X-ray diffraction (XRD) patterns of the as-synthesized samples with nominal compositions of $LiFe_{0.54}Mn_{0.36}P_{0.95}O_{4-\delta}$ and $LiFe_{0.6}Mn_{0.4}PO_4$. The peak positions and intensity ratios of $LiFe_{0.54}Mn_{0.36}P_{0.95}O_{4-\delta}$ are indistinguishable from those of $LiFe_{0.6}Mn_{0.4}PO_4$, suggesting that the crystalline olivine phase in both samples is the same with the off-stoichiometry accommodated as an additional phase. Lattice parameters of $LiFe_{0.54}Mn_{0.36}P_{0.95}O_{4-\delta}$ (a = 10.3648 Å, b = 6.0400 Å, and c = 4.7122 Å) calculated from Rietveld refinement using *Pnma* space group in Fig. 1b also match those of $LiFe_{0.6}Mn_{0.4}PO_4$ (a = 10.3672 Å, b = 6.0407 Å, and c = 4.7138 Å) obtained in this study. The lattice parameters and Rietveld refinement details are summarized in ESI,† Table S1.

Similar full width at half maximum for $LiFe_{0.54}Mn_{0.36}P_{0.95}O_{4-\delta}$ and $LiFe_{0.6}Mn_{0.4}PO_4$ shown in the inset of Fig. 1a implies a similar particle size for both compounds. Indeed, the particle size distribution of $LiFe_{0.54}Mn_{0.36}P_{0.95}O_{4-\delta}$ observed by scanning electron microscopy (SEM) in Fig. 1c is similar to that of $LiFe_{0.6}Mn_{0.4}PO_4$ in Fig. 1d with the average particle size being approximately 40 nm. Note that in both compounds, some particles form secondary agglomerates with the size ranging between 200 and 500 nm. Fig. 1e and f show high resolution transmission electron microscopy (HRTEM) images obtained from $LiFe_{0.54}Mn_{0.36}P_{0.95}O_{4-\delta}$ and $LiFe_{0.6}Mn_{0.4}PO_4$ particles, respectively. Clearly observable lattice fringes indicate well-crystallized olivine phases in both particles. However, the surface morphology noticeably differs from each other: the off-stoichiometric particle is covered with a non-crystalline layer (average 4.5 nm) whereas the surface of the stoichiometric particle is crystalline, as similarly observed in off-stoichiometric $LiFe_{0.9}P_{0.95}O_{4-\delta}$ and $LiMn_{0.9}P_{0.95}O_{4-\delta}$.[22–24] The formation of these amorphous films with self-limiting thickness has been discussed in detail in ref. 24.

In order to analyze the composition of the non-crystalline surface phase, we performed scanning transmission electron microscopy (STEM) electron energy loss spectroscopy (EELS)

[a] *Department of Materials Science and Engineering, Massachusetts Institute of Technology, Cambridge, MA, USA*
[b] *Department of Materials Science and Engineering, Pohang University of Science and Technology (POSTECH), Pohang, Republic of Korea*
[c] *Department of Materials Science and Engineering, University of California, Berkeley, Berkeley, CA, USA. E-mail: gceder@berkeley.edu*

† Electronic supplementary information (ESI) available. See DOI: 10.1039/c5cc04434k

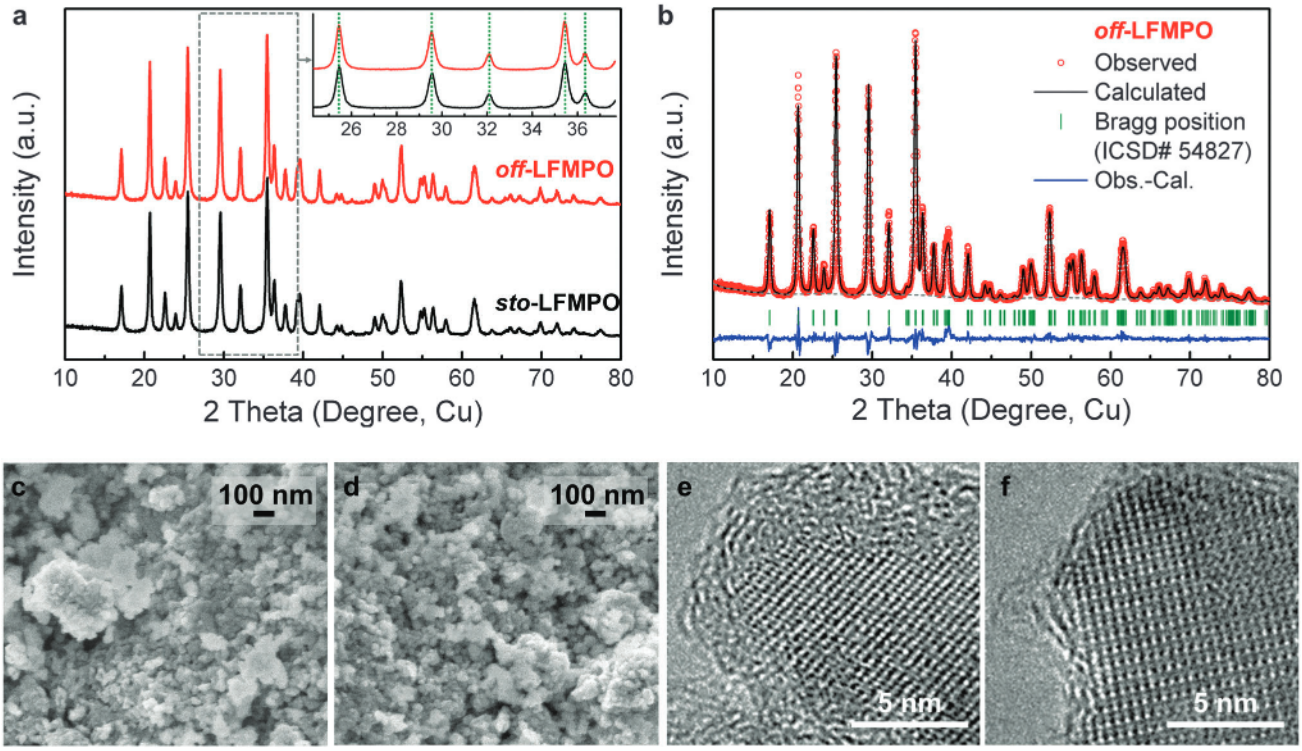

Fig. 1 (a) XRD patterns of $LiFe_{0.54}Mn_{0.36}P_{0.95}O_{4-\delta}$ (off-LFMPO) and $LiFe_{0.6}Mn_{0.4}PO_4$ (sto-LFMPO), (inset) magnified peaks showing their full width at half maximum, (b) Rietveld-refined profile matching of the XRD pattern of $LiFe_{0.54}Mn_{0.36}P_{0.95}O_{4-\delta}$ (off-LFMPO), SEM images of (c) $LiFe_{0.54}Mn_{0.36}P_{0.95}O_{4-\delta}$ and (d) $LiFe_{0.6}Mn_{0.4}PO_4$, HRTEM images of (e) $LiFe_{0.54}Mn_{0.36}P_{0.95}O_{4-\delta}$ and (f) $LiFe_{0.6}Mn_{0.4}PO_4$.

line scanning measurements of P L, O K, Mn L, and Fe L edges across the particle. Fig. 2a and b show HRTEM and the corresponding STEM images of the $LiFe_{0.54}Mn_{0.36}P_{0.95}O_{4-\delta}$ particle, respectively. EELS profiles were collected when electron beams were scanned from the inside of the particle to the non-crystalline surface of the particle along the marked arrow in Fig. 2b. EELS quantification between transition metal L edges and O K edge plotted in Fig. 2c reveals that the (Fe + Mn)/O atomic ratio near the surface region substantially deviates from the ratio of the crystalline bulk region. This indicates that the surface composition is Fe and Mn deficient relatively to the inside of the particle. There is no detectable change for the P/O atomic ratio across the particle within the error bar of EELS quantification (Fig. S1, ESI†), indicating that the surface phases also contain P and O. It should be noted that in some particles weak C K edge is observed (<2 nm) in between the glassy surface and bulk regions, suggesting that the trace amount of carbon remains after firing the carbon-containing precursors.

We also examine the chemical states of P near the surface of the $LiFe_{0.54}Mn_{0.36}P_{0.95}O_{4-\delta}$ particle by X-ray photoelectron spectroscopy (XPS). The P 2p spectrum of $LiFe_{0.54}Mn_{0.36}P_{0.95}O_{4-\delta}$ develops a shoulder around at 134.7 eV as compared with that of $LiFe_{0.6}Mn_{0.4}PO_4$ (Fig. S2, ESI†). This implies that various P states exist in $LiFe_{0.54}Mn_{0.36}P_{0.95}O_{4-\delta}$, and the best fit is indeed obtained by considering P 2p doublets of $LiFe_{0.6}Mn_{0.4}PO_4$ and $Li_4P_2O_7$,[28] as shown in Fig. 2d. The details of the XPS experiment are summarized in Table S2, ESI.†

A computed phase diagram of the Li–Fe–P–O_2 quaternary system suggests that under reducing conditions Fe-deficiency in $LiFe_{0.9}P_{0.95}O_{4-\delta}$ can lead to phase decomposition into

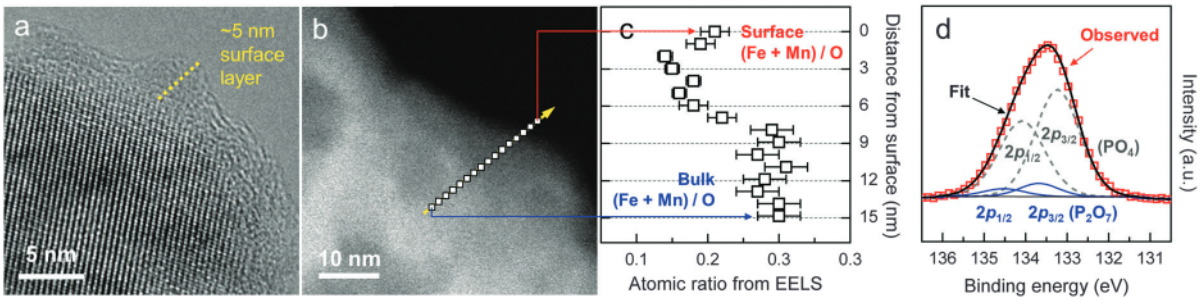

Fig. 2 (a) HRTEM and (b) the corresponding STEM images of $LiFe_{0.54}Mn_{0.36}P_{0.95}O_{4-\delta}$ and (c) atomic ratios of transition metals to oxygen with respect to distance from surface obtained from EELS, and (d) 2p binding energy of P obtained from XPS in $LiFe_{0.54}Mn_{0.36}P_{0.95}O_{4-\delta}$.

stoichiometric $LiFePO_4$ and some phosphates such as $LiPO_3$, $Li_4P_2O_7$ and $LiFeP_2O_7$,[29,30] which agrees with experimental observation.[22,31] A similar conclusion has been drawn for off-stoichiometric $LiMn_{0.9}P_{0.95}O_{4-\delta}$ with slightly different decomposition products: Li_3PO_4, $Li_4P_2O_7$, and $LiMnP_2O_7$.[23,32] Although such a phase diagram is currently unavailable for quinary systems, the decomposition phases of off-stoichiometric $LiFe_{0.54}Mn_{0.36}P_{0.95}O_{4-\delta}$ are likely similar to those of $LiFe_{0.9}P_{0.95}O_{4-\delta}$ and $LiMn_{0.9}P_{0.95}O_{4-\delta}$ as the synthesis environment is almost identical.[22,23] That is, formation of the surface phase can be thermodynamically driven by off-stoichiometry in composition. A more detailed mechanism of why these surface films form and are self-limiting in thickness can be found in the literature.[24] Given the Fe and Mn deficiency detected by EELS, the surface phase may include all or any combinations of $LiPO_3$, Li_3PO_4, $Li_4P_2O_7$, and some Li-phosphates containing Fe and/or Mn in a glassy state.[22,32] Still, due to the non-crystallinity, the existing phosphates likely have a considerable variation in local compositions.

The results shown in Fig. 1 and 2 together point out that the $LiFe_{0.54}Mn_{0.36}P_{0.95}O_{4-\delta}$ particle comprises the crystalline $LiFe_{0.6}Mn_{0.4}PO_4$ particle with the non-crystalline surface of phosphates, balancing the off-stoichiometric ratio. Thus, we can regard $LiFe_{0.54}Mn_{0.36}P_{0.95}O_{4-\delta}$ as basically identical to $LiFe_{0.6}Mn_{0.4}PO_4$ but a compositionally different surface phase.

Fig. 3a–c show voltage *versus* capacity profiles of the $LiFe_{0.54}Mn_{0.36}P_{0.95}O_{4-\delta}$ and $LiFe_{0.6}Mn_{0.4}PO_4$ cathodes in the second cycle. The former reversibly intercalates the theoretical amount of Li (165 mA h g^{-1}) at C/5 in Fig. 3a, achieving 605 W h kg^{-1} calculated by voltage integration of the discharge capacity. This value exceeds the theoretical energy density of $LiFePO_4$ (580 W h kg^{-1}), which is difficult for mixed olivine cathodes to achieve at this rate. In comparison, the stoichiometric cathode does not match the performance: 151 mA h g^{-1} and 558 W h kg^{-1} for specific capacity and energy density, respectively. Moreover, the off-stoichiometric cathode markedly outperforms the stoichiometric one at higher rates: 153 and 135 mA h g^{-1} are obtained at 1C (Fig. 3b) and 5C (Fig. 3c) in $LiFe_{0.54}Mn_{0.36}P_{0.95}O_{4-\delta}$, respectively, but 133 and 88 mA h g^{-1} in $LiFe_{0.6}Mn_{0.4}PO_4$ at the same 1C and 5C. Cycling performance of the $LiFe_{0.54}Mn_{0.36}P_{0.95}O_{4-\delta}$ and $LiFe_{0.6}Mn_{0.4}PO_4$ cathode is excellent, displaying almost no capacity decay after multiple cycles at different rates, as plotted in Fig. 3d. Therefore, $LiFe_{0.54}Mn_{0.36}P_{0.95}O_{4-\delta}$ clearly demonstrates an improved electrochemical performance compared to $LiFe_{0.6}Mn_{0.4}PO_4$.

We further examine the discharge rate capability of $LiFe_{0.54}Mn_{0.36}P_{0.95}O_{4-\delta}$. In Fig. 3e, it delivers 165 mA h g^{-1} at C/5 and 158 mA h g^{-1} at 5C. The achievable capacity decreases as the discharge rate increases: 134, 97, 51, and 25 mA h g^{-1} at 20C, 40C, 60C, and 100C, respectively. In high-rate cycling, electrode configuration influences electrical wiring resistance throughout the cathode and critically determines rate capability.[33,34] Thus, our cathode configuration is altered to include less active materials (35% $LiFe_{0.54}Mn_{0.36}P_{0.95}O_{4-\delta}$) embedded into more electronically conductive matrix (60% carbon black and 5% PTFE binder), thereby ensuring to accommodate large current density with low wiring resistance. Through dilution of the active material, the discharge capacities obtained show immediate enhancement in Fig. 3f: 164 mA h g^{-1} at C/5, 160 mA h g^{-1} at 5C, and 145 mA h g^{-1} at 20C. Most dramatically, 130, 115, and 83 mA h g^{-1} are delivered at higher discharge rates, 40C, 60C, and 100C, respectively.

Compared to stoichiometric $LiFe_{0.6}Mn_{0.4}PO_4$, the larger capacity in off-stoichiometric $LiFe_{0.54}Mn_{0.36}P_{0.95}O_{4-\delta}$ can be explained with better electrical (ionic and electronic) percolation of active particles in the electrode. Nanosized particles often agglomerate with each other, forming substantially larger secondary particles, as observed in $LiFe_{0.54}Mn_{0.36}P_{0.95}O_{4-\delta}$ (Fig. 1c) and $LiFe_{0.6}Mn_{0.4}PO_4$ (Fig. 1d). This agglomeration

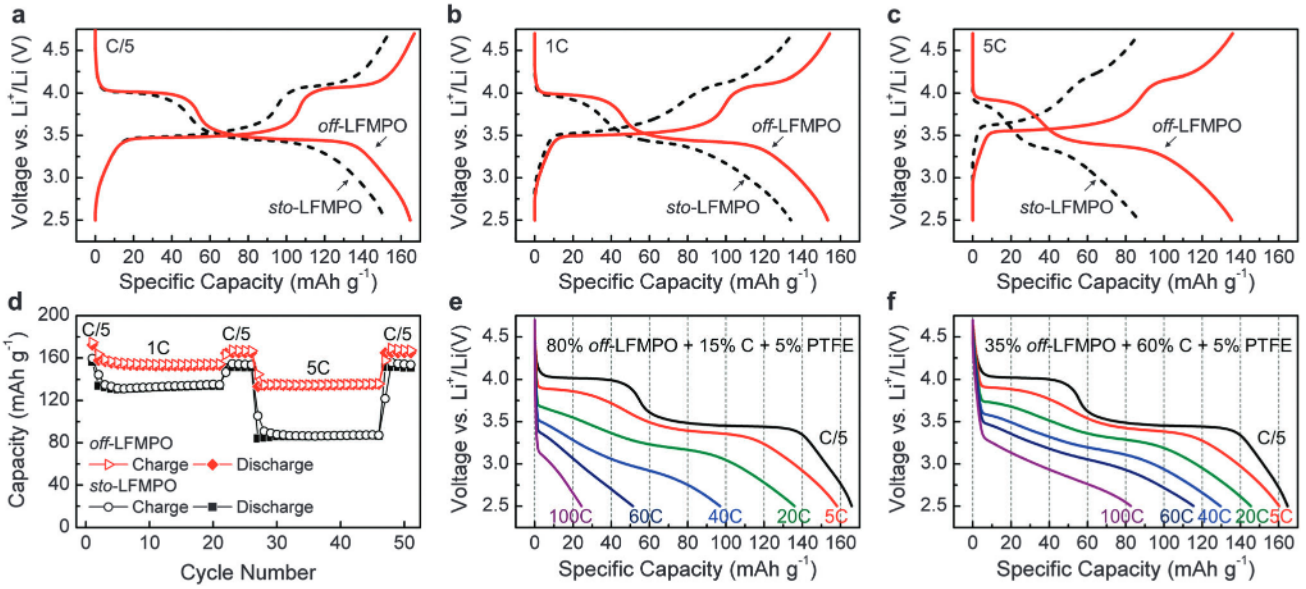

Fig. 3 Voltage versus specific capacity profiles at various rates: (a) C/5, (b) 1C, and (c) 5C. (d) Cyclic performances of $LiFe_{0.54}Mn_{0.36}P_{0.95}O_{4-\delta}$ (off-LFMPO) and $LiFe_{0.6}Mn_{0.4}PO_4$ (sto-LFMPO). Discharge rate capability of (e) undiluted and (f) diluted $LiFe_{0.54}Mn_{0.36}P_{0.95}O_{4-\delta}$ (off-LFMPO).

can leads to incomplete permeation of electrolyte toward the inside, which can apparently reduce accessible capacity.[34–36] The non-crystalline Li phosphates in $LiFe_{0.54}Mn_{0.36}P_{0.95}O_{4-\delta}$ are formed during synthesis, likely encapsulating the primary particle individually. As the phosphate glasses related to $LiPO_3$, Li_3PO_4 and $Li_4P_2O_7$ are known Li^+ conductors,[37–39] they can provide percolated Li^+ transport pathways (*i.e.* ionic wiring) throughout the secondary particles. As a result, Li^+ inside the secondary particle of the off-stoichiometric cathode can be still accessible. This may not be the case for the stoichiometric cathode as it does not have such glassy surface phases. Particle agglomeration can also take an electronic contact away from primary particles to the carbon matrix, resulting in larger charge transfer resistance. The phosphates including transition metal such as Fe^{3+} at the surface and/or the thin residual carbon layer can form an electronic network through the secondary particles and contribute to better wiring in the cathode.[40]

In summary, we synthesized $LiFe_{0.6}Mn_{0.4}PO_4$ with a non-crystalline surface phase by controlling off-stoichiometry and achieved a theoretical capacity of 165 mA h g^{-1} at C/5 cycling and 135 mA h g^{-1} at 5C cycling with good capacity retention. It is also capable of very fast discharging, 115 mA h g^{-1} at 60C and 83 mA h g^{-1} at 100C between 4.7 and 2.5 V, through diluting the cathode active mass. This superior performance likely originates from the phosphate surface layer, which promotes effective electrical wiring for Li^+ transport throughout the cathode. Our off-stoichiometric design strategy is a simple approach to achieve high-rate performance, applicable to other mixed olivine compositions.

Computational resources were provided by the infrastructure of the Materials Project supported by Basic Energy Sciences program of Department of Energy (DOE) under Grant No. EDC-BEE, DOE Contract DE-AC02-05CH11231. The experimental work was supported by the MRSEC Program of the National Science Foundation under award number DMR-0819762 and by the Assistant Secretary for Energy Efficiency and Renewable Energy, Office of Vehicle Technologies of the U.S. DOE under Contract No. DE-AC02-05CH11231, under the Batteries for Advanced Transportation Technologies (BATT) Program.

Notes and references

1 A. K. Padhi, K. S. Nanjundaswamy and J. B. Goodenough, *J. Electrochem. Soc.*, 1997, 144, 1188–1194.
2 A. Yamada, S. C. Chung and K. Hinokuma, *J. Electrochem. Soc.*, 2001, 148, A224–A229.
3 R. Malik, A. Abdellahi and G. Ceder, *J. Electrochem. Soc.*, 2013, 160, A3179–A3197.
4 N. Ravet, Y. Chouinard, J. F. Magnan, S. Besner, M. Gauthier and M. Armand, *J. Power Sources*, 2001, 97–98, 503–507.
5 J. L. Yang, J. J. Wang, Y. J. Tang, D. N. Wang, X. F. Li, Y. H. Hu, R. Y. Li, G. X. Liang, T. K. Sham and X. L. Sun, *Energy Environ. Sci.*, 2013, 6, 1521–1528.
6 Y. J. Lee, H. Yi, W. J. Kim, K. Kang, D. S. Yun, M. S. Strano, G. Ceder and A. M. Belcher, *Science*, 2009, 324, 1051–1055.
7 Y. S. Hu, Y. G. Guo, R. Dominko, M. Gaberscek, J. Jamnik and J. Maier, *Adv. Mater.*, 2007, 19, 1963–1966.
8 S. Y. Chung, J. T. Bloking and Y. M. Chiang, *Nat. Mater.*, 2002, 1, 123–128.
9 Z. H. Chen and J. R. Dahn, *J. Electrochem. Soc.*, 2002, 149, A1184–A1189.
10 J. B. Goodenough and Y. Kim, *Chem. Mater.*, 2010, 22, 587–603.
11 J. M. Tarascon and M. Armand, *Nature*, 2001, 414, 359–367.
12 F. Zhou, M. Cococcioni, K. Kang and G. Ceder, *Electrochem. Commun.*, 2004, 6, 1144–1148.
13 A. Yamada, Y. Kudo and K. Y. Liu, *J. Electrochem. Soc.*, 2001, 148, A1153–A1158.
14 G. H. Li, H. Azuma and M. Tohda, *J. Electrochem. Soc.*, 2002, 149, A743–A747.
15 J. Kim, D. H. Seo, S. W. Kim, Y. U. Park and K. Kang, *Chem. Commun.*, 2010, 46, 1305–1307.
16 D. H. Seo, H. Gwon, S. W. Kim, J. Kim and K. Kang, *Chem. Mater.*, 2010, 22, 518–523.
17 H. Gwon, D. H. Seo, S. W. Kim, J. Kim and K. Kang, *Adv. Funct. Mater.*, 2009, 19, 3285–3292.
18 R. Malik, F. Zhou and G. Ceder, *Phys. Rev. B: Condens. Matter Mater. Phys.*, 2009, 79, 214201.
19 C. Delacourt, L. Laffont, R. Bouchet, C. Wurm, J. B. Leriche, M. Morcrette, J. M. Tarascon and C. Masquelier, *J. Electrochem. Soc.*, 2005, 152, A913–A921.
20 M. Yonemura, A. Yamada, Y. Takei, N. Sonoyama and R. Kanno, *J. Electrochem. Soc.*, 2004, 151, A1352–A1356.
21 A. Yamada, Y. Takei, H. Koizumi, N. Sonoyama, R. Kanno, K. Itoh, M. Yonemura and T. Kamiyama, *Chem. Mater.*, 2006, 18, 804–813.
22 B. Kang and G. Ceder, *Nature*, 2009, 458, 190–193.
23 B. Kang and G. Ceder, *J. Electrochem. Soc.*, 2010, 157, A808–A811.
24 A. Kayyar, H. J. Qian and J. Luo, *Appl. Phys. Lett.*, 2009, 95, 221905.
25 G. Q. Tan, F. Wu, L. Li, R. J. Chen and S. Chen, *J. Phys. Chem. C*, 2013, 117, 6013–6021.
26 K. Sun and S. J. Dillon, *Electrochem. Commun.*, 2011, 13, 200–202.
27 S. D. Xun, J. Chong, X. Y. Song, G. Liu and V. S. Battaglia, *J. Mater. Chem.*, 2012, 22, 15775–15781.
28 W. E. Morgan, W. J. Stec and J. R. Vanwazer, *J. Am. Chem. Soc.*, 1973, 95, 751–755.
29 S. P. Ong, L. Wang, B. Kang and G. Ceder, *Chem. Mater.*, 2008, 20, 1798–1807.
30 The Materials Project webpage, https://materialsproject.org.
31 S. L. Yang, D. N. Wang, G. X. Liang, Y. M. Yiu, J. J. Wang, L. J. Liu, X. L. Sun and T. K. Sham, *Energy Environ. Sci.*, 2012, 5, 7007–7016.
32 S. P. Ong, A. Jain, G. Hautier, B. Kang and G. Ceder, *Electrochem. Commun.*, 2010, 12, 427–430.
33 M. Gaberscek, M. Kuzma and J. Jamnik, *Phys. Chem. Chem. Phys.*, 2007, 9, 1815–1820.
34 P. A. Johns, M. R. Roberts, Y. Wakizaka, J. H. Sanders and J. R. Owen, *Electrochem. Commun.*, 2009, 11, 2089–2092.
35 J. Chong, S. D. Xun, X. Y. Song, P. Ridgway, G. Liu and V. S. Battaglia, *J. Power Sources*, 2012, 200, 67–76.
36 H. Q. Li and H. S. Zhou, *Chem. Commun.*, 2012, 48, 1201–1217.
37 S. W. Martin, *J. Am. Ceram. Soc.*, 1991, 74, 1767–1784.
38 B. Wang, B. S. Kwak, B. C. Sales and J. B. Bates, *J. Non–Cryst. Solids*, 1995, 183, 297–306.
39 P. Dabas, V. Subramanian and K. Hariharan, *J. Mater. Sci.*, 2014, 49, 134–141.
40 K. C. Sobha and K. J. Rao, *J. Non–Cryst. Solids*, 1996, 201, 52–65.

